

## **Radiative Processes and Geometry of Spectral States of Black-hole Binaries**

A. A. Zdziarski

*N. Copernicus Astronomical Center, Bartycka 18, 00-716 Warszawa,  
Poland*

**Abstract.** I review radiative processes responsible for X-ray emission in the hard (low) and soft (high) spectral states of black-hole binaries. The main process in the hard state appears to be thermal Comptonization (in a hot plasma) of blackbody photons emitted by a cold disk. This is supported by correlations between the spectral index, the strength of Compton reflection, and the peak frequencies in the power-density spectrum, as well as by the frequency-dependence of Fourier-resolved spectra. Spectral variability may then be driven by the variable truncation radius of the disk. The soft state appears to correspond to the smallest truncation radii. However, the lack of high-energy cutoffs observed in the soft state implies that its main radiative process is Compton scattering of disk photons by nonthermal electrons. The bulk-motion Comptonization model for the soft state is shown to be ruled out by the data.

### **1. Introduction**

Black-hole (hereafter BH) binaries show two main states in their X-ray/ $\gamma$ -ray (hereafter  $X\gamma$ ) spectra: a hard (also called low) one and a soft (also called high) one. The two states differ in the relative strength of the blackbody and power-law-like components, as illustrated by the case of Cyg X-1 in Figure 1 (Gierliński et al. 1999 [G99]). Apart from these two, an intermediate state (also shown in Figure 1) and an off state simply correspond to a transition period between the hard and the soft state, and to a very weak X-ray emission, respectively. Finally, a very high state is distinguished by both the above components being strong.

In this work, I will concentrate on radiative processes dominant during the hard and soft states. I will also discuss implications of correlations among the spectral and timing properties for the source geometry.

### **2. The Hard State**

#### **2.1. Thermal Comptonization**

Thermal Comptonization of soft blackbody photons, as the radiative process expected to dominate in a hot accretion disk surrounded by a cold one, was proposed to take place in BH binaries by Eardley, Lightman, & Shapiro (1975) and Shapiro, Lightman, & Eardley (1976). (That geometry was also proposed by Thorne & Price 1975.) Shapiro et al. (1976) obtained a solution for spectral

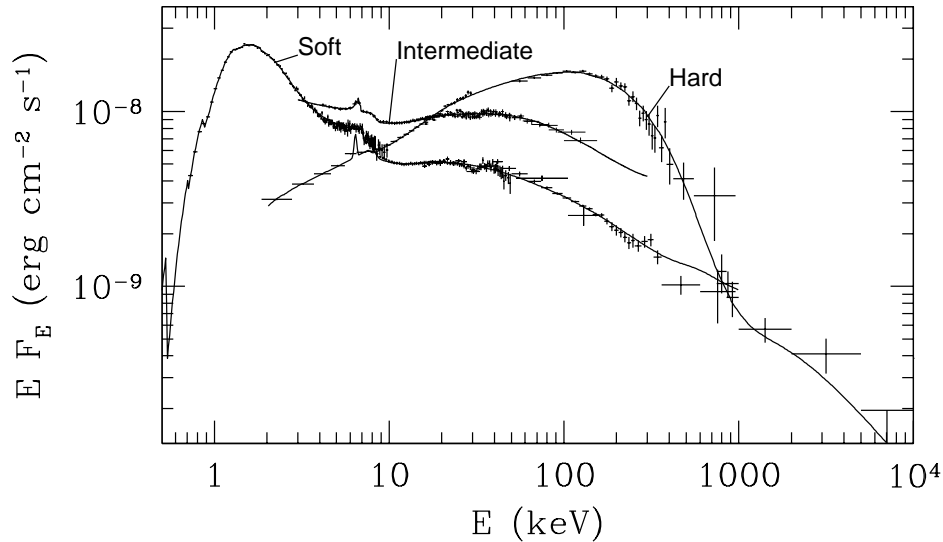


Figure 1. Energy spectra in three states of Cyg X-1.

formation in this process and found it to qualitatively agree with the high-energy cutoff seen in balloon data for Cyg X-1. Then, Sunyaev & Trümper (1979) (and later some other authors) fitted hard X-ray data from Cyg X-1 using the optically-thick, nonrelativistic, Comptonization solution of Sunyaev & Titarchuk (1980). That fit neglected the presence of a Compton-reflection spectral component not known at that time (see §2.2 below). This, most likely, explains their fitted value of the electron temperature of  $kT = 27$  keV, which is much lower than the values of  $\sim 100$  keV obtained in contemporary models (e.g., Gierliński et al. 1997). The effect is due to the spectral curvature in the hard X-ray regime being partly due to Compton reflection, as pointed out by Haardt et al. (1993). This can be seen in Figure 2 by comparing the total spectrum, curved in the  $\sim 15$ – $100$  keV range, with the Comptonization component, rather flat in that range.

Presently, the best evidence that the primary  $X\gamma$  continua of BH binaries in the hard state are due to thermal Comptonization comes from observations by the CGRO/OSSE detector simultaneous with X-ray observations by other instruments. The obtained plasma parameters are  $kT \simeq 50$ – $100$  keV and a Thomson optical depth of  $\tau_T \sim 1$  (in agreement with the values of Shapiro et al. 1976). These parameters have been obtained, e.g., for the hard state of Cyg X-1 (Figure 1, Gierliński et al. 1997) and GX 339-4 (Figure 2, Zdziarski et al. 1998 [Z98], and in preparation); in addition, they appear consistent with the spectra of transient BH binaries (Grove et al. 1998 [G98]).

The photon spectral index,  $\Gamma$ , of the primary X-ray continuum is a function of  $\tau_T$  and  $kT$ ; roughly, it depends on them through the Compton parameter,  $y \equiv 4(kT/m_e c^2)\tau_T$ . At a given  $\tau_T$ ,  $kT$  is determined by balance between heating

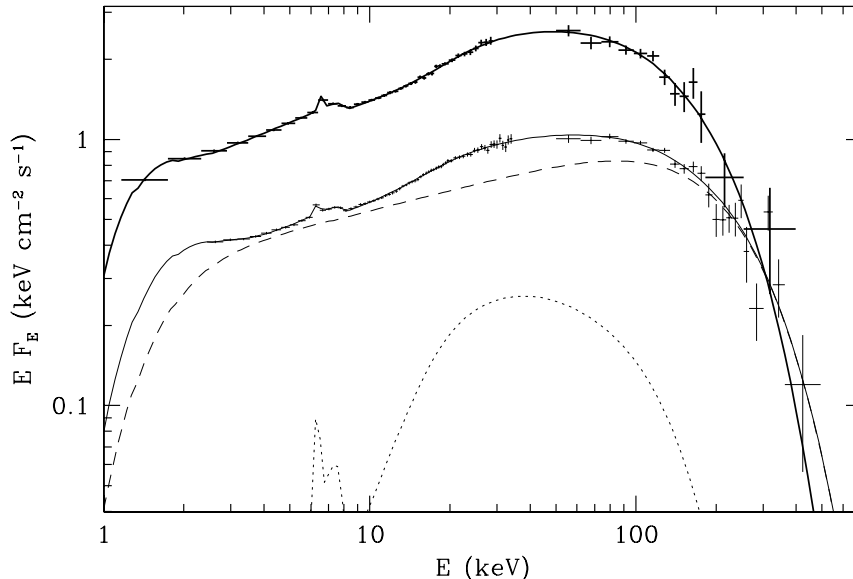


Figure 2. X $\gamma$  spectra of GX 339–4 in the hard state from simultaneous observations by *Ginga*-OSSE (upper spectrum: Z98) and RXTE-OSSE (lower spectrum: Zdziarski et al., in preparation). The spectra are fitted by the sum of blackbody, thermal Comptonization, and Compton reflection including an Fe K $\alpha$  line. The last two components are shown for the lower spectrum by the dashed and dotted curves, respectively.

of the plasma and its radiative cooling, with the cooling rate proportional to the flux of soft photons providing seeds for Comptonization. Then, the stronger the flux in the soft photons is, the larger  $\Gamma$  is (e.g., see Beloborodov 1999b).

The two spectra of GX 339–4 shown in Figure 2 have almost identical X-ray spectral slopes (corresponding to a constant  $y$ ), but the fitted electron temperature increases from  $kT \simeq 50$  to  $\sim 80$  keV when the luminosity,  $L$ , is smaller by a factor of  $\sim 2$ . A similar behaviour (but for a smaller range of  $L$ ) is seen in four spectra of Cyg X-1 presented in Gierliński et al. (1997). A constant  $\Gamma$  (or  $y$ ) implies an approximately constant geometry (determining the amplification factor of Comptonization, see §2.2 below). Then, a higher  $kT$  at a lower  $L$  corresponds to a proportionally smaller  $\tau_T$ . Such a behaviour is expected in hot accretion disks (Shapiro et al. 1976; Abramowicz et al. 1995; Narayan & Yi 1995), in which  $\tau_T$  decreases with decreasing  $\dot{m}$  ( $\equiv \dot{M}c^2/L_E$ ). Then, the character of the  $\tau_T(L)$  dependence may allow us to determine which branch of the hot disk solution, advection-dominated or cooling-dominated, is followed by the source. Hot disks parametrized by  $y$  were studied by Zdziarski (1998), whose

results applied to GX 339–4 appear to favour the advection-dominated solution branch (Zdziarski et al., in preparation).

## 2.2. Compton Reflection and its Correlation with Spectral and Timing Properties

As illustrated in Figure 2, the  $X\gamma$  spectra of BH binaries usually show a distinct component due to Compton reflection (Lightman & White 1988; Magdziarz & Zdziarski 1995) of the primary continuum from a cold medium, presumably an optically-thick accretion disk (Done et al. 1992; Gierliński et al. 1997; Z98; Życki, Done, & Smith 1998; 1999; Done & Życki 1999; Gilfanov, Churazov, & Revnivtsev 1999 [GCR99]; Revnivtsev, Gilfanov, & Churazov 1999; 2000 [RGC00]).

A very interesting property of Compton reflection is that its relative strength,  $R$  ( $\sim \Omega/2\pi$ , where  $\Omega$  is the solid angle of the reflector as seen from the hot plasma), strongly correlates with the spectral and timing properties of the sources. Ueda, Ebisawa, & Done (1994) have found a correlation between  $R$  and  $\Gamma$  in GX 339–4, albeit based on a few observations with relatively large errors. Then, Zdziarski, Lubiński, & Smith (1999 [ZLS99]) have shown the presence of a strong  $R$ - $\Gamma$  correlation at a very high statistical significance in 47 *Ginga* observations of Seyfert 1s. Also, 23 *Ginga* observations of BH and neutron-star binaries were found to obey the same correlation (Zdziarski 1999 [Z99]).

The correlation has recently been unambiguously confirmed in the RXTE data on Cyg X-1 and GX 339–4. It is seen both in spectra obtained at different epochs and in Fourier-resolved spectra (i.e., corresponding to variability in a given range of Fourier frequencies) of a given observation (Revnivtsev et al. 1999; GCR99; RGC00). Figure 3 presents the RXTE results for those two objects and GS 1354–644 (M. Gilfanov, private comm.), as well as the *Ginga* results for 20 observations of three BH binaries (Z99).

Furthermore, GCR99 and RGC00 find that the strength of Compton reflection strongly correlates with the characteristic frequencies in the power-density spectrum (PDS), both in Cyg X-1 and GX 339–4. Their PDS per logarithm of frequency exhibit two peaks at frequencies,  $f$ , which correlate positively with both  $R$  and  $\Gamma$  (with the ratio of the two peak frequencies remaining constant). Also, the spectra from both reflection and Fe  $K\alpha$  fluorescence are smeared, with the amount of smearing increasing with  $R$  and  $\Gamma$  (RGC00).

A likely general explanation of the  $R$ - $\Gamma$  correlation appears to be a mutual interaction between a hot, thermal plasma and a cold medium, as proposed by ZLS99. Namely, the cold medium both reflects the hot-plasma emission and provides blackbody photons as seeds for Comptonization. Then, the larger the solid angle subtended by the reflector is, the stronger the flux of soft photons is, and, consequently, the stronger the cooling of the plasma is. In the case of thermal plasma (§2.1), the stronger the cooling by seed photons incident on the plasma is, the softer the resulting X-ray power law spectrum is.

ZLS99 considered 2 specific models: one with a central, hot disk surrounded by a cold disk, and one with bulk motion in a disk corona. Here, we discuss only the former model (see Beloborodov 1999a, b for discussion of the latter). In this model, the surrounding cold disk is assumed to extend from some large, outer radius down to such a (variable) transition radius that it may overlap with the

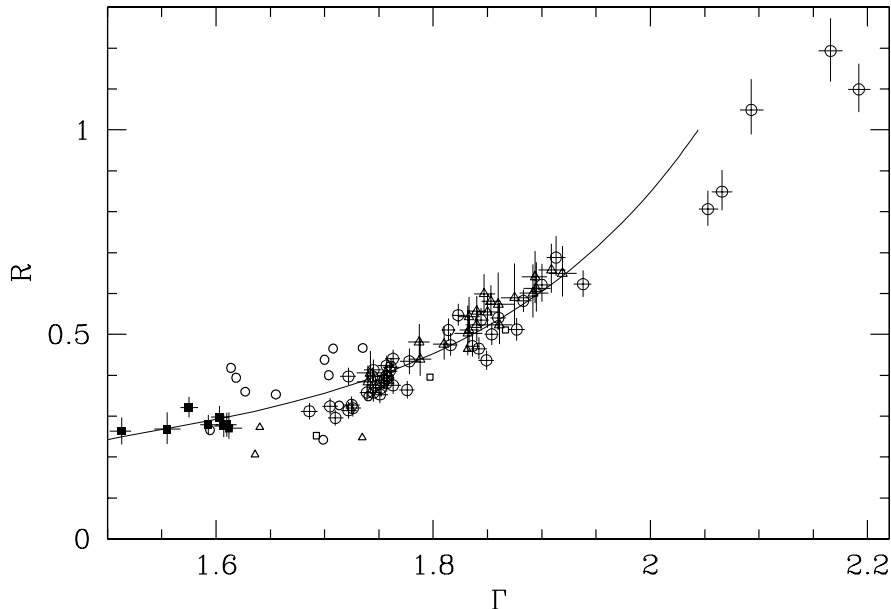


Figure 3. Correlation between the strength of Compton reflection and the X-ray spectral index in BH binaries. Larger symbols with error bars and smaller ones without them correspond to observations by RXTE and *Ginga*, respectively. Open circles, triangles, squares, and filled squares correspond to Cyg X-1, GX 339-4, Nova Muscae, and GS 1354-644, respectively. The solid curve corresponds to the model of ZLS99 in the geometry shown in Figure 4.

hot disk (see also Poutanen, Krolik, & Ryde 1997), as shown in Figure 4. Then, the more inward the cold disk extends, the stronger Compton reflection is, the softer the Comptonization spectrum is (see above), and the higher the characteristic frequencies of the system are. The solid curve in Figure 3 corresponds to this model with the parameters of ZLS99. (Note that their soft photon energy is probably too low for the BH-binary case; on the other hand, other effects not included in that highly idealized model may also affect the values of  $R$ .) We see that it provides an excellent description of the data.

Note that the interpretation in terms of blackbody cooling is also in agreement with a theoretical prediction that thermal synchrotron emission provides a negligible flux of seed photons for Comptonization in luminous BH binaries (Wardziński & Zdziarski 2000). However, the thermal synchrotron process can be important at low luminosities, in which case departures from the  $R$ - $\Gamma$  correlation are expected (which effect might explain the soft spectrum with weak reflection seen in a low- $L$  state of GS 2023+338: Życki et al. 1999).

On the other hand, detailed interpretation of the correlation of  $R$  with the peak PDS frequencies is probably not straightforward. Here, we simply

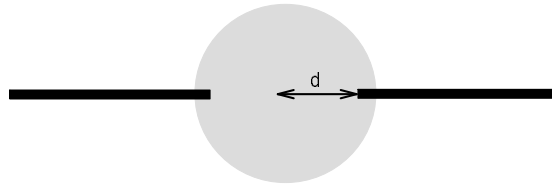


Figure 4. The geometry with a central, hot plasma surrounded by a cold disk (ZLS99). The cold disk partly enters the hot plasma down to the radius  $d$  which determines the spectral hardness and the amount of reflection, resulting in the correlation shown in the solid curve in Figure 3.

compare the characteristic PDS frequencies with the Keplerian one, which is likely to represent an upper limit on the characteristic frequencies of physical processes taking place at a given radius. We can define the Keplerian radius,  $r_K(f)GM/c^2$ ,

$$r_K(f) \simeq 10^3 [m(f/1 \text{ Hz})]^{-2/3}, \quad (1)$$

where  $M = mM_\odot$ . For the higher of the peak PDS frequencies in Cyg X-1,  $f \sim 0.5\text{--}3 \text{ Hz}$  (GCR99),  $r_K \sim 100\text{--}300$ , which may represent an upper limit on the range of radii responsible for that peak. This is then in agreement with the transition radii of  $r \sim 20\text{--}50$  found for the hard state of Cyg X-1 by Done & Zycki (1999) by assuming that the observed smearing is solely due to Doppler and gravitational effects on the surface of a cold disk. We note, however, the result of Revnivtsev et al. (1999) that a given observed spectrum is a sum of spectra with *different* values of  $R$  and  $\Gamma$  corresponding to different Fourier frequencies. Then, fitting such a sum by a single power law plus reflection will result in some smearing of the reflection in addition to Doppler/gravity effects. Therefore, the transition radii of Done & Zycki (1999) may underestimate the actual values.

The Fourier-resolved spectra show a positive correlation between  $R$  and  $\Gamma$  (Revnivtsev et al. 1999; RGC00); also, the hardest spectra with the weakest reflections correspond to the highest Fourier frequencies. Although this is an opposite effect to the positive correlation of  $R$  and  $\Gamma$  with the peak frequencies in the PDS spectra, it can also be explained by the hot/cold disk model discussed above. Namely, the spectra corresponding to the highest Fourier frequencies presumably originate close to the central BH where both the blackbody flux from the outer cold disk and the solid angle subtended by it are small. The hardest/weakest-reflection spectra shown by Revnivtsev et al. correspond to  $f \lesssim 30 \text{ Hz}$ , which then correspond to  $r_K \gtrsim 20$  (at  $m = 10$ ).

Still, a realistic representation of the geometry will certainly be much more complex than the sketch in Figure 4. In particular, a major issue involves implications of the observed time lags of harder X-rays with respect to softer ones (see Cui 1999 for a recent review).

### 3. The Soft State

X $\gamma$  spectra in the soft state can be roughly described by a strong blackbody component dominating energetically, followed by a high-energy tail with  $\Gamma \sim 2.5$ – $3$ ; see Figure 1. The blackbody component comes, most likely, from an optically-thick accretion disk. On the other hand, there is no consensus at present regarding the origin of the tail. Three main models have been proposed, all involving Comptonization of blackbody photons by high-energy electrons. The models differ in the distribution (and location) of the electrons, which are assumed to be either thermal (with a Maxwellian distribution), nonthermal (with a distribution close to a power law), or in free fall from about the minimum stable orbit down to the horizon of the black hole.

A crucial test of the models is given by how they are able to reproduce the shape of the high-energy tail. Its major spectral feature is the lack of an observable high-energy cutoff in all BH binaries in the soft state observed so far (G98; Tomsick et al. 1999; G99; E. Grove, private comm.). In two objects with the best soft  $\gamma$ -ray data, GRO J1655–40 and GRS 1915+105, the power-law tail extends above  $\sim 0.5$  MeV without any cutoff (G98; Tomsick et al. 1999; see §3.3 below). Also, the spectrum of the tail, at least in some well-studied cases, contains a component due to Compton reflection and Fe K $\alpha$  fluorescence (Cyg X-1: G99, GCR99; GRO J1655–40: Tomsick et al. 1999; GRS 1915+105: Coppi 1999; Nova Muscae 1991: Życki et al. 1998; 1999).

#### 3.1. Thermal Comptonization

Thermal Comptonization was proposed to model spectra of the soft state of Cyg X-1 (Poutanen et al. 1997; Cui et al. 1998; Esin et al. 1998) and other BH binaries (Miyamoto et al. 1991; Esin, McClintock, & Narayan 1997). This model can, in principle, account for the X-ray part of the spectra. However, very high plasma temperatures are then required to account for the observed steep power-law tails extending to  $\sim 1$  MeV, which then requires  $\tau_T \ll 1$  in order to keep the spectrum soft. This, in turn, causes distinct scattering profiles from consecutive orders of scattering to be visible in the spectrum (see Figure 7 of Coppi 1999) which are not seen in the soft-state data. For instance, a deep dip in the spectrum above the blackbody component is predicted by this model, whereas the Cyg X-1 data show instead an excess of photons in that region, resulting in a very bad fit of this model (G99). Thus, existing observations rule out this model in its simplest version with a single plasma component dominating the formation of the tail.

On the other hand, the observed spectra can be possibly reproduced by a suitable distribution of  $T$  and  $\tau_T$ . Such models are, in general, difficult to rule out. However, they appear to require a fine-tuning of the  $(T, \tau_T)$  distribution. This is because a range of  $T$  from nonrelativistic to relativistic values is required to account for the broadband tails, and Comptonization in those two regimes has different properties—especially, the energy gain per scattering is  $\propto T$  and  $T^2$ , respectively. Then, a power-law distribution of  $T$  would still result in a curved spectrum, most likely contrary to observations.

### 3.2. Bulk-motion Comptonization

Another model of bulk-motion Comptonization (hereafter abbreviated as BMC; Blandford & Payne 1981; Colpi 1988) was proposed to account for the soft-state, power-law spectra by Chakrabarti & Titarchuk (1995). In their model, an accretion flow passes through a shock at a radius close to the radius ( $r_{\text{ms}}$ ) of the minimum stable orbit, and it becomes quasi-spherical at smaller radii. Above the shock, the flow consists of a geometrically-thin, optically-thick accretion disk (as required by the observations of strong blackbody components) and an optically-thin flow above and below the disk. (Note that in the standard accretion-disk model, the disk passes through a sonic point close to  $r_{\text{ms}}$  without a shock and remains geometrically-thin to the horizon; e.g., see Muchotrzeb & Paczyński 1982.)

Then, the free-falling electrons acquire velocities of  $v \sim c$  close to the horizon, and Comptonization using the large bulk inflow velocity of the electrons (as opposed to their assumed smaller thermal motions) gives rise to a power-law spectrum. The power-law index,  $\Gamma$ , depends on  $\dot{m}$  as shown, e.g., by Monte-Carlo calculations of Laurent & Titarchuk (1999 [LT99]). It decreases with increasing  $\dot{m}$ , and  $\Gamma \lesssim 3$  is achieved for  $\dot{m} \gtrsim 2$ ; see Figure 5.

A very attractive feature of the BMC model is that it links the presence of the high-energy tail to the lack of a hard surface for a BH. Free-falling electrons can achieve relativistic velocities only close to the BH horizon, unlike the case of accretion onto a neutron star. Indeed, no strong high-energy tails have been observed as yet from accreting neutron stars in their high states (although power-law spectra with  $\Gamma \sim 2.5$  and no observable high-energy cutoff have been seen, usually in low- $L$  states; e.g., see Barret et al. 1992; Goldwurm et al. 1996; Harmon et al. 1996; Piraino et al. 1999). Note that the free-falling electrons represent, in fact, an advection-dominated flow (with the distinction of the transition radius being at  $r_{\text{ms}}$ ), models of which also link certain features of BH accretion to the lack of a hard stellar surface (e.g., Narayan & Yi 1995).

However, the attractiveness of a model is not equivalent to its proof, and we should look for specific predictions of the model that can be confronted with data. The main such specific model prediction is the energy of a high-energy cutoff. Based on a nonrelativistic comparison of Compton upscattering and recoil, Ebisawa, Titarchuk, & Chakrabarti (1996) predicted a sharp cutoff at  $E/m_e c^2 \sim \dot{m}^{-1}$ . Given that  $\dot{m} \gtrsim 2$ , as required by  $\Gamma \lesssim 3$ , is typically observed, this cutoff would be significantly below 0.5 MeV. In addition, a cutoff or a break around  $m_e c^2$  is expected regardless of the value of  $\dot{m}$  due to relativistic effects. First, the Klein-Nishina cross-section decreases with energy ( $\sigma_{\text{KN}} \simeq 0.4\sigma_{\text{T}}$  at  $m_e c^2$  in the electron rest frame), which results in a spectral curvature. Second, photons with energies around  $m_e c^2$  are produced relatively close to the horizon, which results in only backscattered photons (whose energy is much less than the average energy after scattering) escaping the flow due to light bending. A related effect is that the escaping electrons scattered close to the horizon will have their energies strongly reduced by the gravitational redshift.

All those effects have been taken into account in the Monte Carlo simulations, in the Schwarzschild metric, of LT99, whose work fully confirms the considerations above. Indeed, *all* model spectra shown by LT99 have sharp high-energy cutoffs above  $\sim 100$  keV, with the flux at 200 keV being  $\lesssim 0.5$  below the

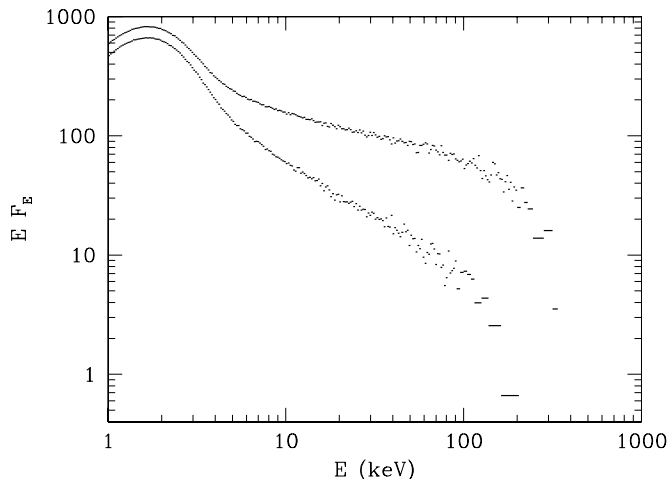


Figure 5. Spectra in the BMC model simulated by LT99 (statistical errors are comparable to the scatter of the points). The lower and upper spectra correspond to  $\dot{m} = 2$  and 4, respectively. The free-falling electrons were assumed to have  $kT = 5$  and 20 keV, and the power-law parts of the spectra have  $\Gamma \simeq 2.9$  and 2.5, respectively.

extrapolation of the high-energy power law, as illustrated in Figure 5. This is also in agreement with the presence of sharp cutoffs at  $\sim 200$  keV obtained in BMC models of Titarchuk, Mastichiadis, & Kylafis (1997) and Psaltis & Lamb (1999).

On the other hand, no high-energy cutoff has been yet discovered in the soft state of BH binaries. In particular, the OSSE spectra show no trace of any break around  $\sim 100$ – $200$  keV in the cases of the soft state of Cyg X-1 (G99), GRS 1915+105, GRS 1009–45, 4U 1543–47, GRS 1716–249, and GRO J1655–40 (G98). A spectrum of the last object from G98 (accumulated over  $\sim 30$  observing days) is shown in Figure 6. We clearly see no hint of a cutoff up to at least 600 keV. More recent data show no cutoff to even higher energies (E. Grove, private comm.).

This lack of a cutoff is clearly incompatible with the BMC spectra. This is illustrated in Figure 6, which also shows the theoretical spectrum of LT99 for  $\dot{m} = 2$ . This spectrum matches well the low-energy slope of the OSSE spectrum, but then shows a sharp cutoff with no photons found in the simulation above 200 keV. This strongly rules out the BMC model.

We note that this conclusion has not been reached by proponents of this model because they have performed no fits to the OSSE data. Shrader & Titarchuk (1998) fitted observations of GRO J1655–40 and GRS 1915+105 from RXTE/PCA, whose high-quality data extend up to  $\lesssim 50$  keV only. They also fitted data from CGRO/BATSE, which instrument does not have a sufficient sensitivity to constrain the spectra at  $\gtrsim 100$  keV. Parenthetically, we note that their shown models have no high-energy break up to  $\sim 300$  keV, contrary to

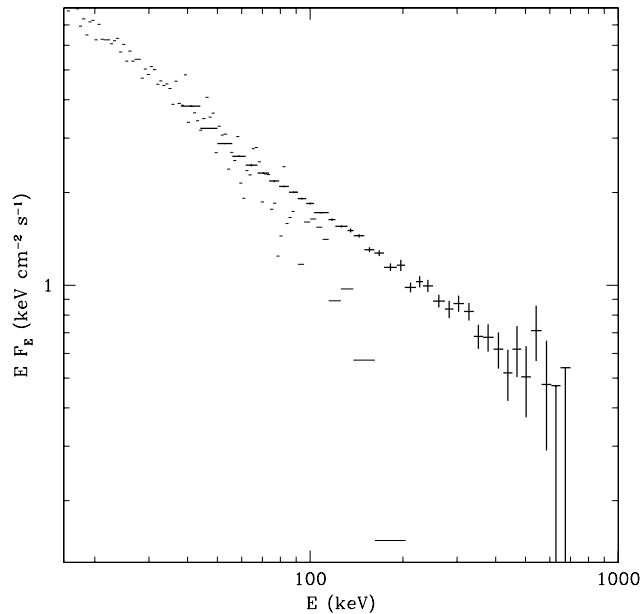


Figure 6. The OSSE spectrum of GRO J1655–40 (crosses) compared to the prediction of the BMC model (thin horizontal lines).

their reference to models of Titarchuk et al. (1997) which have a sharp cutoff at  $\sim 200$  keV. Then, Borozdin et al. (1999) fitted RXTE data of the above 2 objects, as well as of XTE J1755–324 and GRS 1739–278, and *Exosat*/GSPC data of EXO 1846–031. The usable energy ranges of all those data extend to  $\lesssim 100$  keV (see Figure 1 in Borozdin et al. 1999) and thus cannot be used to test the BMC model. Borozdin et al. (1999) do show OSSE data for two 6-day observing periods of GRO J1655–40 and for an observation of XTE J1755–324, but they do not present any fits to them. Finally, Shrader & Titarchuk (1999) fitted RXTE/PCA data for LMC X-1 and *Ginga* data for Nova Muscae 1991, both of which extend to energies  $\lesssim 30$  keV. In summary, all of the fitted data are insensitive to the presence or absence of the spectral breaks predicted by the BMC model to occur at  $\sim 100$ – $200$  keV.

In addition to the main problem of the high-energy cutoff, the BMC model appears to have a number of other problems when confronted with data. One issue involves the predicted dependence  $\Gamma(\dot{m})$ . It can be compared to the soft-state data for Cyg X-1, for which  $\dot{m} \simeq 0.5$  and the observed  $\Gamma \sim 2.5$  (G99). On the other hand, Table 2 in LT99 gives  $\Gamma = 3.8$  at this  $\dot{m}$ , i.e., a much softer spectrum than observed. Thus, unless advection strongly dominates in the soft state of Cyg X-1 and the actual  $\dot{m} \gtrsim 4$ , the BMC model is ruled out in this case, independent of the evidence from the lack of an observed high-energy cutoff.

On the other hand, a significant hardening of the slope can be obtained if the free-falling electrons also have thermal motion with a high enough temperature. Results of LT99 (see their Table 2) show that the slope can be hardened by

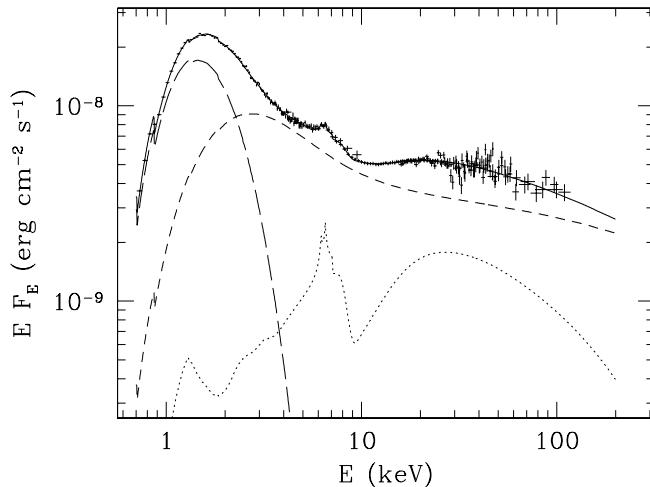


Figure 7. The soft-state spectrum of Cyg X-1 from an ASCA-RXTE observation fitted by Comptonization by nonthermal electrons (dominating above the break seen in the short-dashed curve at  $\sim 15$  keV) as well as by thermal ones (the short-dashed curve below the break), of disk blackbody photons (long dashes), and Compton reflection from the disk (dots).

$\Delta\Gamma \sim 1$  if  $kT = 50$  keV. However, the spectral formation is then almost fully due to thermal Comptonization, and although the BMC process is still taking place, its role is negligible. For example, at  $\dot{m} = 2$ , an increase of  $kT$  from 5 keV (when BMC dominates) to 50 keV leads to an increase of the photon flux at 100 keV by a factor of  $\sim 100$  (see Figures 4 and 6 in LT99)—an effect entirely due to Compton scattering on electrons with velocities dominated by their thermal motion. This thermal-Comptonization model can still be ruled out for the soft state based on the energy of its high-energy cutoff (see §3.1 above).

Another problem for the BMC model (as well as for any model with the source of the hard emission located below  $\sim r_{\text{ms}}$ ) is the detection of Compton reflection in the soft-state spectra of GRO J1655–40 (Tomsick et al. 1999), GRS 1915+105 (Coppi 1999), Nova Muscae (Życki et al. 1998; 1999), and Cyg X-1 (G99; GCR99); see Figure 7. In objects which show state transitions, the strength of Compton reflection is *highest* in the soft state (GCR99; Życki et al. 1998; 1999) and usually consistent with  $\Omega \sim 2\pi$  (G99; Coppi 1999). This is clearly incompatible with the geometry of the BMC model, in which a thin disk is outside the central, spherical inflow (see Figure 2 in LT99).

Chakrabarti & Titarchuk (1995) have addressed this problem by proposing that the observed reflection-like features are due to partial covering by an absorbing medium with  $\tau_{\text{T}} \sim 3$ . An absorbing medium has been detected in GRO J1655–40 at a distance  $\sim 10^{10}$  cm but with  $\tau_{\text{T}} \sim 0.2$  only (Ueda et al. 1998). This low  $\tau_{\text{T}}$  cannot explain the observed reflection features. On the other hand, as noted by Chakrabarti & Titarchuk (1995), the Fe  $K\alpha$  line will be

very weak at  $\tau_T \sim 3$  (results of Makishima 1986 imply an equivalent width of  $\sim 10$  eV), whereas the data show lines with typical equivalent widths  $\gtrsim 100$  eV (Życki et al. 1998; Tomsick et al. 1999; G99). Furthermore, those data show broadening of the Fe K $\alpha$  line, implying that most of the reflection takes place from an inner disk, and arguing against disk flaring as a possible explanation of the large reflection fraction.

Another issue to be considered is time lags of harder X-rays with respect to softer ones observed in the soft state (Cui et al. 1997; Li, Feng, & Chen 1999; Cui 1999) as well as in the hard state. In the hard state, those lags have been interpreted as due to either delays between consecutive Compton scatterings in a halo with a large size,  $r \gtrsim 10^4$  (Kazanas, Hua, & Titarchuk 1997; Hua, Kazanas, & Titarchuk 1997), spectral evolution of a disk-corona system (Poutanen & Fabian 1999), or drift of blobs in a hot disk (Böttcher & Liang 1999). The lags in the soft state are shorter than those in the hard state but still reach  $\gtrsim 10$  ms for photons in the tail with respect to the blackbody-peak photons in the case of Cyg X-1 (Figure 8 in Cui et al. 1997; Figure 5 in Li et al. 1999; Figure 2 in Cui 1999). On the other hand, a characteristic time lag expected due to scattering in a converging flow below  $\sim r_{\text{ms}}$  is  $\sim 0.2$  ms, i.e., much less than that observed.

Thus, the BMC model can be rejected based on the observed absence (in all objects with data extending to soft  $\gamma$ -rays) of a high-energy cutoff around  $\sim 100$ – $200$  keV. This cutoff is *the* specific prediction of the BMC model, making it highly testable. Furthermore, the model disagrees with data on some predictions related to its geometry of a central, very compact source—notably on those regarding the Fe K features and timing properties.

Naturally, the problems discussed above can be solved by assuming that the scattering electrons have sufficiently high nonthermal velocities, that the size of the source is much larger than  $r_{\text{ms}}$ , and that there is a significant overlap between the hot plasma and the cold disk (which possibilities are mentioned by LT99). Then, however, the spectral formation will be due to Compton scattering by electrons with velocities dominated by their nonthermal motion, with their bulk motion playing a negligible role, and the model will lose its identity and become virtually indistinguishable from the nonthermal corona model (described below).

### 3.3. Nonthermal Comptonization

The spectral constraints discussed above strongly point to (1) a radiative process capable of producing power-law spectra with no cutoffs up to  $\sim 1$  MeV, and (2) a geometry with a large solid angle subtended by the reflector as measured from the source of the power-law emission. Natural candidates for that radiative process and geometry are single Compton scattering of the blackbody photons by power-law electrons, and a disk-corona geometry, respectively. Such a model has been proposed by Poutanen & Coppi (1998) and developed in detail and tested against Cyg X-1 data by G99 (using the code of Coppi 1999).

The model consists of a corona above a standard, optically-thick accretion disk. Selected electrons from a thermal distribution in the corona are accelerated to relativistic energies, possibly in reconnection events. The relativistic electrons Compton upscatter the disk photons, forming the high-energy tail. The relativistic electrons also transfer some of their energy via Coulomb scattering to the thermal electrons (at the lowest energies of the total distribution), heating them

to a temperature much above the Compton temperature. The thermal electrons then also efficiently upscatter the disk photons (in addition to nonthermal upscattering), which process forms the excess below  $\sim 10$  keV observed in Cyg X-1; see Figure 7. The radiation of the corona is also partly Compton-reflected from the disk, as observed (Figure 7).

An important parameter of the coronal plasma is its compactness, i.e., the ratio of the luminosity to size. At a high compactness, copious  $e^\pm$  pairs are produced in photon-photon collisions, which then leads to a distinct pair-annihilation feature (e.g., see Svensson 1987). Such a feature is not seen, which constrains the compactness from above. At a low compactness, Coulomb energy losses of relativistic electrons become dominant over the Compton losses. This leads to a break in the steady-state distribution of relativistic electrons. This, in turn, leads to a corresponding break in the photon spectrum. Again, such a break is not seen, which constrains the compactness from below. In the case of Cyg X-1, the allowed range of compactnesses corresponds to a characteristic size of the order of tens of  $GM/c^2$  (G99). This corresponds to the range of radii at which most of the accretion energy is dissipated.

Note that this characteristic size is also in agreement with the timing data of Cyg X-1 in the soft state. The break frequency in the PDS spectrum is at 13–14 Hz (Cui et al. 1997), which corresponds to the Keplerian frequency at  $r \sim 40$  (at  $m = 10$ ); see Equation (1). Also, the 6.5–13 keV photons are observed to lag the 2–6.5 keV ones by  $\sim 2$  ms on average (over the 1–10 Hz Fourier periods; see Figure 9 in Cui et al. 1997). These two energy ranges are dominated by upscattering of disk photons by the thermal part of the electron distribution (G99); see Figure 7. If this time lag is interpreted as being due to light-travel delays in a scattering medium, the resulting characteristic size is  $r \sim 40$ , as well. Furthermore, the location of the corona at such radii is also consistent with the observed broadening of the Fe  $K\alpha$  line in Cyg X-1 (G99).

Another parameter of interest is the power-law index,  $p$ , of the rate of electron acceleration. Its value determines the photon index of the high-energy tail via the relation  $p \simeq 2(\Gamma - 1)$  (taking into account the steepening of the electron distribution due to the energy loss). Then, the typical value of  $\Gamma$  being  $\sim 2.5$  implies that the acceleration in the corona proceeds at a rate  $\propto \gamma^{-3}$ .

The relative normalization of the tail with respect to the blackbody implies, from energy balance, the fraction of the accretion power released in the corona. In the case of Cyg X-1, it is  $\sim 0.5$ . Also, the disk in the soft state of Cyg X-1 is found to be gas-pressure dominated all the way to  $r_{\text{ms}}$  and, thus, stable (G99).

This nonthermal model has been successfully fitted to soft-state spectra of Cyg X-1 measured by ASCA, RXTE, and OSSE (G99) and by *BeppoSAX* (Frontera et al. 2000), as well as to RXTE data on GRS 1915+105 by Coppi (1999). Figures 1 and 7 present fits to Cyg X-1 data from ASCA, RXTE, and OSSE (G99).

#### 4. Comparison with AGNs and Neutron Stars

X-ray spectra of Seyferts show power-law indices and reflection components rather similar to those of BH binaries in the hard state, as illustrated in Figure 8. It shows results from *Ginga* (ZLS99) as well as some RXTE fit results for

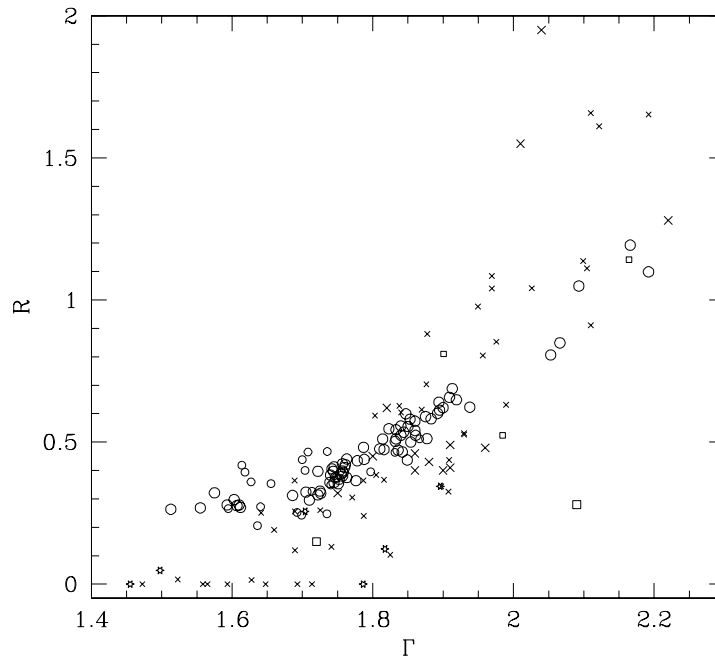


Figure 8. Values of  $\Gamma$  and  $R$  in the hard state of BH binaries (open circles; same as in Figure 3) and neutron-star binaries (open squares), in Seyfert 1s (crosses) and broad-line radio galaxies (asterisks). Large and small symbols correspond to RXTE and *Ginga* data, respectively. For clarity, error bars are not shown.

MCG-6-30-15 (Lee et al. 1998), MCG-5-23-16 (Weaver, Krolik, & Pier 1998), NGC 5548 (Chiang et al. 2000), and IC 4329A (Done, Madejski, & Smith 2000).

We see that the popular notion that Compton reflection is weaker in BH binaries than in Seyferts is not confirmed by the data shown here. Specifically, BH binaries with hard spectra have stronger Compton-reflection components than Seyfert 1s with the same  $\Gamma$  (in the range  $\Gamma \lesssim 1.8$ ). This is equivalent to AGNs having softer spectra at a given  $R$ . This effect can be explained by the difference in typical blackbody temperatures between BH binaries and AGNs. For a given amplification factor (presumably controlled by geometry), higher blackbody temperatures (in BH binaries) result in harder X-ray spectra (see Figure 10 in Z99).

We also see that Seyferts show much more scatter than BH binaries on the  $R$ - $\Gamma$  diagram. This may be related to a wider range of physical conditions in Seyferts than in BH binaries. For instance, molecular tori in Seyferts are likely to contribute to reflection without a noticeable effect on the cooling of the central, hot plasma, which might explain objects with  $R > 1$ . On the other hand, outflows (Beloborodov 1999a, b) may explain the weakness of reflection in some objects, especially broad-line radio galaxies (Woźniak et al. 1998; Z99); see Figure 8.

Then, Seyfert 1s with soft spectra and strong reflection, like MCG-6-30-15, may represent AGN counterparts of the soft state of BH binaries (as discussed in Done et al. 2000). On the other hand, those counterparts may be given by Narrow-Line Seyfert 1s, as proposed by Pounds, Done, & Osborne (1995), although their timing properties appear to be different from each other.

Typical plasma temperatures in Seyferts are relatively poorly determined (e.g., see Z99; Done et al. 2000), but they still appear similar to  $kT$  in BH binaries. In particular, the Seyfert with the best-known soft  $\gamma$ -ray spectrum, NGC 4151 (Johnson et al. 1997), has an (intrinsic) average  $X\gamma$  spectrum virtually identical to the *Ginga*-OSSE spectrum of GX 339-4 shown in Figure 2 (Z98). Then, the similarity of the values of both  $\Gamma$  and  $kT$  implies similar values of  $\tau_T$  ( $\sim 1$ ).

Among neutron-star binaries, the class closest to BH binaries is that of Type 1 X-ray bursters, which are characterized by disk accretion at a relatively low  $\dot{m}$  and by magnetic fields weak enough not to dominate the dynamics of accretion. Between thermonuclear bursts, they show two spectral states, low (hard) and high (soft), similarly to BH binaries. The spectral and timing properties of BH binaries and X-ray bursters are relatively similar, as recently discussed by Barret et al. (2000). The main differences are that the X-ray spectra of bursters in the low state are, *on average*, softer (with  $\Gamma \gtrsim 1.9$ ) than those of BH binaries. They also show Compton reflection components with a range of  $R$  and roughly obeying the  $R$ - $\Gamma$  correlation; see Figure 8. This figure shows the RXTE data for GS 1826-238 and SLX 1735-269 (Barret et al. 2000) and *Ginga* data for GS 1826-238 and 4U 1608-522 (ZLS99).

When fitted by thermal Comptonization, bursters in the low state usually show high-energy cutoffs corresponding to  $kT \lesssim 30$  keV, whereas BH binaries have  $kT \gtrsim 50$  keV (Z98; Barret et al. 2000). However, there are cases of low-state spectra of bursters extending above  $\sim 100$  keV without a measurable cutoff, e.g., 4U 0614+091 (Piraino et al. 1999) and SAX J1810.8-2609 (Natalucci et al. 2000), which seems to happen for relatively soft power laws with  $\Gamma \gtrsim 2$ . In the case of 4U 0614+091, the power law is accompanied by reflection with  $R \gtrsim 1$  showing a strong  $R$ - $\Gamma$  correlation, but offset to  $\Gamma \sim 2.4$ -3 (Piraino et al. 1999), which  $\Gamma$  is similar to those seen in the soft state of BH binaries (§3).

## 5. Conclusions

1. The main radiative process in the hard state of BH binaries is thermal Comptonization with  $kT \sim 50$ -100 keV and  $\tau_T \sim 1$ .
2. The relative strength of Compton reflection correlates with the X-ray spectral index and with peak frequencies in the PDS spectrum. The simplest interpretation of these correlations appears to be in terms of a cold accretion disk overlapping with a central, hot disk.
3. Models of the power-law tail in the soft state in terms of thermal and bulk-motion Comptonization are shown to be ruled out by the data. An alternative, successful model involves Compton scattering by nonthermal electrons in a corona.

4.  $X\gamma$  spectra of BH binaries in the hard state are very similar to those of Seyfert 1s, although the latter show more diversity in their spectral properties.
5.  $X\gamma$  spectra of BH binaries in the hard state have, *on average*, harder X-ray power laws and higher high-energy cutoffs (corresponding to  $kT \gtrsim 50$  keV) than those of X-ray bursters.

**Acknowledgments.** This research has been supported in part by a grant from the Foundation for Polish Science and the KBN grants 2P03C00511p0(1,4) and 2P03D00614. I thank Marat Gilfanov, Eric Grove, and Philippe Laurent for providing me with their results in numerical form, and Andrei Beloborodov, Chris Done, Juri Poutanen, and Lev Titarchuk for valuable comments.

## References

- Abramowicz, M. A., Chen, X., Kato, S., Lasota, J.-P., & Regev, O. 1995, *ApJ*, 438, L37
- Barret, D., et al. 1992, *ApJ*, 394, 615
- Barret, D., Olive, J. F., Boirin, L., Done, C., Skinner, G. K., & Grindlay, J. E. 2000, *ApJ*, 533, 329
- Beloborodov, A. M. 1999a, *ApJ*, 510, L123
- Beloborodov, A. M. 1999b, in *ASP Conf. Ser. Vol. 161, High Energy Processes in Accreting Black Holes*, eds. J. Poutanen & R. Svensson (San Francisco: ASP), 295
- Blandford, R. D., & Payne, D. G. 1981, *MNRAS*, 194, 1041
- Borozdin, K., Revnivtsev, M., Trudolyubov, S., Shrader, C., & Titarchuk, L. 1999, *ApJ*, 517, 367
- Böttcher, M., & Liang, E. P. 1999, *ApJ*, 511, L37
- Chakrabarti, S. K., & Titarchuk, L. G. 1995, *ApJ*, 455, 623
- Chiang, J., Reynolds, C. S., Blaes, O. M., Nowak, M. A., Murray, N., Madejski, G. M., Marshall, H. L., & Magdziarz, P. 2000, *ApJ*, 528, 292
- Colpi, M. 1988, *ApJ*, 326, 223
- Coppi, P. S. 1999, in *ASP Conf. Ser. Vol. 161, High Energy Processes in Accreting Black Holes*, eds. J. Poutanen & R. Svensson (San Francisco: ASP), 375
- Cui, W. 1999, in *ASP Conf. Ser. Vol. 161, High Energy Processes in Accreting Black Holes*, eds. J. Poutanen & R. Svensson (San Francisco: ASP), 97
- Cui, W., Ebisawa, K., Dotani, T., & Kubota, A. 1998, *ApJ*, 493, L75
- Cui, W., Zhang, S. N., Focke, W., & Swank, J. H. 1997, *ApJ*, 484, 383
- Done, C., Madejski, G. M., & Życki, P. T. 2000, *ApJ*, in press
- Done, C., Mulchaey, J. S., Mushotzky, R. F., & Arnaud, K. A. 1992, *ApJ*, 395, 275
- Done, C., & Życki, P. T. 1999, *MNRAS*, 305, 457
- Eardley, D. M., Lightman, A. P., & Shapiro, S. L. 1975, *ApJ*, 199, L153

- Ebisawa, K., Titarchuk, L., & Chakrabarti, S. K. 1996, PASJ, 48, 59
- Esin, A. A., McClintock, J. E., & Narayan, R. 1997, ApJ, 489, 865
- Esin, A. A., Narayan, R., Cui, W., Grove, J. E., & Zhang, S.-N. 1998, ApJ, 505, 854
- Frontera, F., Palazzi, E., Zdziarski, A. A., et al. 2000, ApJ, submitted
- Gierliński, M., Zdziarski, A. A., Done, C., Johnson, W. N., Ebisawa, K., Ueda, Y., Haardt, F., & Phlips, B. F. 1997, MNRAS, 288, 958
- Gierliński, M., Zdziarski, A. A., Poutanen, J., Coppi, P., Ebisawa, K., & Johnson, W. N. 1999, MNRAS, 309, 496 (G99)
- Gilfanov, M., Churazov, E., & Revnivtsev, M. 1999, A&A, 352, 182 (GCR99)
- Goldwurm, A., et al. 1996, A&A, 310, 857
- Grove, J. E., Johnson, W. N., Kroeger, R. A., McNaron-Brown, K., & Skibo, J. G. 1998, ApJ, 500, 899 (G98)
- Haardt, F., Done, C., Matt, G., & Fabian, A. C. 1993, ApJ, 411, L95
- Harmon, B. A., Wilson, C. A., Tavani, M., Zhang, S. N., Rubin, B. C., Paciesas, W. S., Ford, E. C., & Kaaret, P. 1996, A&AS, 120, C197
- Hua, X.-M., Kazanas, D., & Titarchuk, L. 1997, ApJ, 482, L57
- Johnson, W. N., McNaron-Brown, K., Kurfess, J. D., Zdziarski, A. A., Magdziarz, P., & Gehrels, N. 1997, ApJ, 482, 173
- Kazanas, D., Hua, X.-M., & Titarchuk, L. 1997, ApJ, 480, 735
- Laurent, P., & Titarchuk, L. 1999, ApJ, 511, 289 (LT99)
- Lee, J. C., Fabian, A. C., Reynolds, C. S., Iwasawa, K., & Brandt, W. N. 1998, MNRAS, 300, 583
- Li, T. P., Feng, Y. X., & Chen, L. 1999, ApJ, 521, 789
- Lightman, A. P., & White, T. R. 1988, ApJ, 335, 57
- Magdziarz, P., & Zdziarski, A. A. 1995, MNRAS, 273, 837
- Makishima, K. 1986, in *The Physics of Accretion onto Compact Objects*, eds. K. O. Mason, M. G. Watson, & N. E. White (Berlin: Springer), 249
- Miyamoto, S., Kimura, K., Kitamoto, S., Dotani, T., & Ebisawa, K. 1991, ApJ, 383, 784
- Muchotrzeb, B., & Paczyński, B. 1982, Acta Astron., 32, 1
- Narayan, R., & Yi, I. 1995, ApJ, 452, 710
- Natalucci, L., Bazzano, A., Cocci, M., Ubertini, P., Heise, J., Kuulkers, E., in 't Zand, J. J. M., & Smith, M. J. S. 2000, ApJ, 536, in press
- Piraino, S., Santangelo, A., Ford, E. C., & Kaaret, P. 1999, A&A, 349, L77
- Pounds, K. A., Done, C., & Osborne, J. P. 1995, MNRAS, 277, L5
- Poutanen, J., & Coppi, P. S. 1998, Physica Scripta, T77, 57
- Poutanen, J., & Fabian, A. C. 1999, MNRAS, 306, L31
- Poutanen, J., Krolik, J. H., & Ryde, F. 1997, MNRAS, 292, L21
- Psaltis, D., & Lamb, F. K. 1999, in ASP Conf. Ser. Vol. 161, *High Energy Processes in Accreting Black Holes*, eds. J. Poutanen & R. Svensson (San Francisco: ASP), 410
- Revnivtsev, M., Gilfanov, M., & Churazov, E. 1999, A&A, 347, L23

- Revnivtsev, M., Gilfanov, M., & Churazov, E. 2000, *A&A*, in press (RGC00)
- Shapiro, S. L., Lightman, A. P., & Eardley, D. M. 1976, *ApJ*, 204, 187
- Shrader, C. R., & Titarchuk, L. 1998, *ApJ*, 499, L31
- Shrader, C. R., & Titarchuk, L. 1999, *ApJ*, 521, L121
- Sunyaev, R. A., & Titarchuk, L. G. 1980, *A&A*, 86, 121
- Sunyaev, R. A., & Trümper, J. 1979, *Nature*, 279, 506
- Svensson, R. 1987, *MNRAS*, 227, 403
- Thorne, K. S., & Price, R. H. 1975, *ApJ*, 195, L101
- Titarchuk, L., Mastichiadis, A., & Kylafis, N. D. 1997, *ApJ*, 487, 834
- Tomsick, J. A., Kaaret, P., Kroeger, R. A., & Remillard, R. A. 1999, *ApJ*, 512, 892
- Ueda, Y., Ebisawa, K., & Done, C. 1994, *PASJ*, 46, 107
- Ueda, Y., Inoue, H., Tanaka, Y., Ebisawa, K., Nagase, F., Kotani, T., & Gehrels, N. 1998, *ApJ*, 492, 782
- Wardziński, G., & Zdziarski, A. A. 2000, *MNRAS*, 314, 183
- Weaver, K. A., Krolik, J. H., & Pier, E. A. 1998, *ApJ*, 498, 213
- Woźniak, P. R., Zdziarski, A. A., Smith, D., Madejski, G. M., & Johnson, W. N. 1998, *MNRAS*, 299, 449
- Zdziarski, A. A. 1998, *MNRAS*, 296, L51
- Zdziarski, A. A. 1999, in *ASP Conf. Ser. Vol. 161, High Energy Processes in Accreting Black Holes*, eds. J. Poutanen & R. Svensson (San Francisco: ASP), 16, astro-ph/9812449 (Z99)
- Zdziarski, A. A., Lubiński, P., & Smith, D. A. 1999, *MNRAS*, 303, L11 (ZLS99)
- Zdziarski, A. A., Poutanen, J., Mikołajewska, J., Gierliński, M., Ebisawa, K., & Johnson, W. N. 1998, *MNRAS*, 301, 435 (Z98)
- Zdziarski, A. A., et al., in preparation
- Życki, P. T., Done, C., & Smith, D. A. 1998, *ApJ*, 496, L25
- Życki, P. T., Done, C., & Smith, D. A. 1999, *MNRAS*, 305, 231